HAL
open science

Measuring Changes in Wettability and Surface Area during Micro Droplet Corrosion Measurements

Samantha Michelle Gateman, Oumaïma Gharbi, Mireille Turmine, Vincent Vivier

To cite this version:

Samantha Michelle Gateman, Oumaïma Gharbi, Mireille Turmine, Vincent Vivier. Measuring Changes in Wettability and Surface Area during Micro Droplet Corrosion Measurements. Electrochimica Acta, 2021, 399, pp.139402. 10.1016/j.electacta.2021.139402 . hal-03377329

HAL Id: hal-03377329

https://hal.science/hal-03377329v1

Submitted on 14 Oct 2021

HAL is a multi-disciplinary open access archive for the deposit and dissemination of scientific research documents, whether they are published or not. The documents may come from teaching and research institutions in France or abroad, or from public or private research centers.

L'archive ouverte pluridisciplinaire **HAL**, est destinée au dépôt et à la diffusion de documents scientifiques de niveau recherche, publiés ou non, émanant des établissements d'enseignement et de recherche français ou étrangers, des laboratoires publics ou privés.

Journal Pre-proof

Measuring Changes in Wettability and Surface Area during Micro Droplet Corrosion Measurements

Samantha Michelle Gateman,* Oumaïma Gharbi,* Mireille Turmine, and Vincent Vivier

Sorbonne Université, CNRS, Laboratoire Interfaces et Systèmes Electrochimiques, UMR 8235, 4 Place Jussieu, 75005, Paris, France

Sorbonne Université, CNRS, Laboratoire de Réactivité de Surface UMR 7197, 4 Place Jussieu, 75005, Paris, France

Samantha.gateman@sorbonne-universite.fr

oumaima.gharbi@sorbonne-universite.fr

Journal Pre-proof

Abstract

We report a new method for directly monitoring dynamic surface wetting that occurs during electrochemical droplet cell corrosion measurements on an Al alloy and Cu galvanic couple. The combination of a goniometer and potentiostat enabled the *in situ* observation of wettability during polarization of each metal and at the interface in 0.4 μL NaCl aqueous droplets. Droplet spreading was heterogeneously dynamic for measurements at the interface of the two metals, where oxygen from the surrounding environment diffused into the droplet edges and reduced on the cathodic metal, thus increasing the wettability on this region, while the anodic metal served as a sacrificial

anode and remained in a constant wetted state. Such dynamic wetting was inhibited by performing measurements under anaerobic conditions, where minimal changes in voltammetric response were observed. All voltammetry was normalized by the true surface area of the droplet footprint, which was measured after droplet evaporation instead of overestimating the corrosion current densities by using the pipette aperture. This work highlights the potential for the combined goniometer-electrochemical setup to further enhance the corrosion community's knowledge about interfacial chemistry and the importance of considering the dynamic evolution of micro/nanoscale droplets on heterogeneous substrates when estimating corrosion rates.

Keywords

Corrosion, Electrochemical droplet cell, Surface chemistry, Wettability, Micro electrochemistry

1. Introduction

Restricting the surface area of working electrodes for micro electrochemical measurements is crucial for microanalysis and for better understanding the role of the interface texture on the electrochemical response. Electrochemical droplet cell (EDC) methodologies utilize a micro/nano capillary/pipette to create a miniaturized electrochemical cell at the tip of the aperture to enable direct and highly localized electrochemical measurements. The conception of the micro droplet cell in 1995 by Bohni et al. was presented as a method to measure localized corrosion at individual inclusions present in stainless steels with high spatial resolution.[1] The original three-electrode setup consisted of a micro capillary mounted onto an optical microscope,

Journal Pre-proof

enabling rough control of the cell positioning relative to the substrate. The pipette aperture size varied from 1 to 1000 µm by controlling the pulling parameters of the micro capillaries, hence varying and controlling the surface area of the working electrode.[1–3]

The current obtained during corrosion polarization measurements must be normalized by the working electrode's surface area to extract corrosion parameters and to make comparisons between different measurements on different areas/materials. In traditional macroscale corrosion experiments, the surface area of the sample is typically governed by the working electrode opening of the electrochemical cell used to expose a pre-defined region. While using EDC methodologies with large pipette apertures, growth of the droplet is possible due to the pressure of the electrolyte reservoir and the wettability of the interface.[4,5] In order to maintain droplet size, hence the working electrode's surface area, silicon rubber gaskets around the pipette tips were implemented to successfully isolate the working electrode's surface area and avoid droplet spreading.[2,6,7]

Current droplet cell techniques (known as scanning electrochemical cell microscopy (SECCM), or scanning micropipette contact method (SMCM)) have upgraded the manual positioning system to automatic step motors and piezo electrics for a more accurate and systematic approach.[8] This change has enabled the use of smaller pipette apertures (<100 nm), where the droplet volume is not affected by the reservoir pressure, but hangs from the pipette aperture without growth, therefore mitigating the need for a silicon gasket. It has been shown that the surface area defined by the droplet is related to the pipette aperture.[7] However, unlike in traditional macroscale methods, there is no

Journal Pre-proof

mechanism that maintains the droplet size throughout analysis, and therefore the surface area can become dynamic. For instance, solvent evaporation from the nano/micro droplet can greatly change the local electrolyte concentration, affecting the measured electrochemical response or even halt due to crystallization. Such issue has been minimized in recent efforts, including using solvents with a low vapour pressure,[9–11] performing measurements under a thin layer of oil,[12,13] and utilizing a humidity chamber.[14] Although these methods have discouraged evaporation, such solutions pose other challenges. For instance, some proposed environments do not represent classical corroding systems (i.e., neutral pH, high salt concentrations, exposed to air), can induce corrosion inhibition behavior that is not representative of the true metal-interface chemistry, or can increase noise due to air flow induced from the cycling of humid/dry environments.

Changes in surface energy/wettability due to polarization and/or reactivity can also impact the wetted surface being evaluated. The change in water contact angle (WCA) brings forth information regarding the interaction between the liquid and the substrate. AC electrochemical measurements and WCA values were previously performed inside of a small droplet on a model system (i.e., a well-characterized redox system on Pt) to study the local electrochemical behavior of a solid-liquid interface.[15] In the case of a corroding system, polarization can induce the formation/breakdown of a surface film, alter the adsorption layer on the electrode's surface, and alter topography (leading to an increase in surface roughness), all of which will affect the measured surface wettability, and hence surface area, throughout the electrochemical measurement. Such changes in

Journal Pre-proof

surface area can influence the extracted current density, especially on the micro and nanoscale. Furthermore, when a droplet is in contact with two dissimilar materials, for instance, at the boundary between the metal matrix and a microstructural feature of an alloy, the surface energy, hence wettability, of each surface can be different, and droplet spreading can be heterogeneous. Nonetheless, up-to-date SECCM/SMCM corrosion studies do not take into account, nor measure, the true surface area nor fluctuations between analyzed regions. Instead, either non-normalized currents are reported,[12,16] or the pipette aperture measured via electron microscopy is taken as the static estimated surface area for all points analyzed.[9,10,14,16,17]

In this work, we have combined a goniometer and a potentiostat to investigate wettability *in situ* while performing electrochemical measurements within a micro liter droplet on an Al alloy and Cu galvanic couple. Such couple was chosen because Al alloys are attractive for many industrial sectors that require high strength and low density infrastructure, while Cu is a common alloying additive in Al alloys and tends to form precipitates within the metal matrix.[19–22] Changes in wettability, hence WCA values, are measured *in situ* through a camera. This impacts the surface area of the working electrode over the course of a measurement, which is measured *ex situ* via microscopy and is used to normalize current instead of the pipette aperture for a more accurate extraction of corrosion current density.

This setup directly observes changes in wettability during polarization, thus enabling corrosion scientists to visualize droplet dynamics and changes in surface energy in real

Journal Pre-proof

time. By investigating the behavior of a pure metal, an alloy, and at the interface of two dissimilar metallic materials, we aim to simulate EDC measurements performed at the interface of microstructural features and metal matrices in order to understand droplet dynamics and corrosion chemistry at such interfaces.

2. Experimental

2.1. Materials and Reagents

The 0.05 M NaCl electrolyte (VWR Prolabo chemicals, Belgium) was prepared using Elga ultrapure water (Veolia, France). Pure Cu and Al alloy 7475-T761 were electrically connected to illustrate the difference in electrochemical reactivity encountered in many alloy systems. The Al 7475-T761/Cu couple was prepared by mechanically forcing a 11 mm diameter cylinder of Cu into the center of a 20 mm diameter cylinder of Al 7475-T761 that had a drilled hole the same diameter as the Cu cylinder in its center. It was confirmed previously that no crevices were present between the two materials via optical microscopy.[23] A metallic pin was attached to the back of the sample to act as the electrical connector and then the entire system was mounted in electrically insulating resin. The sample was polished in ethanol using a series of SiC grinding/polishing pads, where the last polish was performed using 2400 grit. The polishing procedure used was chosen to clearly observe the droplet footprint and to a have reproducible surface preparation procedure. However, it may be of interest to apply the method outlined here to real-world samples, which are frequently characterized to possess heterogeneous surface morphology. For such in-lab experiments, the samples must be flat (in

Journal Pre-proof

comparison to the droplet size) to avoid droplet hysteresis and movement, and the sample under investigation must be small enough to fit the dimensions of the goniometer used.

The sample was left for 24h to create a stable oxide film on both metals. Surface roughness influences wettability and hence water contact angle values. The effect of surface roughness, as well as surface chemistry, on different metals' wettability is of great interest while performing EDC corrosion measurements and is currently being investigated as a follow up study of the work presented here.

2.2. Water Contact Angle Measurements

All water contact angle experiments were performed using a programmable DSA100E drop shape analyser (KRÜSS, Hamburg, Germany) using the software, Advance (KRÜSS, Hamburg, Germany). The 0.05 M NaCl droplet volume was 0.4 μL and the dosing rate was 16 μL/s. This was the smallest droplet volume that could be dispensed reproducibly using a stainless-steel flat needle (3.65 cm in length) with an inner and outer diameter of 275 ± 1 μm and 491 ± 2 μm, respectively, with minimal deformation. Both the dosing height (i.e., the height at which a droplet was dispensed from the needle far from the substrate) and deposit height (i.e., the height of the needle when the droplet made contact with the substrate) was set and held constant throughout all measurements. Water contact angle values were systematically calculated using an ellipse model.

WCA measurements were first performed on a glass slide to measure the rate of evaporation in order to evaluate at which scan rate potentiodynamic polarization (PDP) should be performed. Measurements were carried out with (Figure 1A) and without

Journal Pre-proof

(Figure 1B) the steel needle to observe the effect of the electrolyte reservoir inside the syringe, as the needle is in contact with the droplet throughout the electrochemical measurements. The needle/droplet approach speed towards the substrate was observed to be about 0.5 mm/s. The height of the needle when the droplet was in contact with the surface (deposit height) was set so that the WCA values recorded for the needle in contact with the droplet were the same as for a free droplet (i.e., without the needle in contact). This minimized the deformation of the droplet due to pressure from the needle, which could alter the WCA values recorded. Measurements on glass were performed at least 10 times for statistical analysis, where the average value and associated error at 95% confidence are reported. All measurements were performed in a temperature-controlled room fixed at 23°C in Paris in May with a relative humidity (R.H) of ~60%.

As time increased, the shape of the droplet changed and the volume decreased, indicating that the pressure of the reservoir did not induce droplet growth. After 4 minutes the droplet completely evaporated while not in contact with the electrolyte reservoir. Although the droplet was still present when in contact with the needle, the diameter of the droplet significantly decreased, indicating that much of the solvent evaporated. Due to the fast evaporation rate, all electrochemical measurements were performed and complete within the first minute of contact.

Measurements were then performed on the metal sample. The three regions of interest for investigation were identified as: pure Cu, Al alloy, and at the interface of the two metals. At least 3 replicates were done for each region. It should be noted that only one

Journal Pre-proof

measurement at the interface was positioned so that the camera could capture the WCA on the two different metals. The needle was in contact with the droplet for 30s before raising it to the dosing height in order to simulate the same setup used to perform electrochemical measurements. The OCP values were not extracted from these experiments. The droplets completely evaporated before transfer of the sample for *ex situ* optical microscopy, where the corroded/salt footprints on the surface enabled the extraction of exposed surface area.

2.3. Electrochemical Setup and Validation

All electrochemical measurements were performed using a Gamry Instruments Reference 600+ potentiostat (Lyon, France) using a two-electrode setup, as seen in the schematic shown in Figure 2A, and using the Gamry Instruments Framework software. The goniometer's droplet dispensing needle (Figure 2B) was utilized as the quasi reference counter electrode (QRCE) as it was fabricated of stainless steel. The surface area of the needle was 29.8 mm^2, which was obtained by adding the surface areas of the region inside the needle (circumference of the inner diameter multiplied by the length of the needle) and the tip of the needle in contact with the droplet (subtracting the area of the inner circle from the outer circle). As a result, the QRCE was ~17x larger than the largest droplet footprint. The open circuit potential (OCP) of the needle was measured for 10 min with respect to a commercial Ag/AgCl saturated reference electrode to ensure stability (Figure 2C). The average OCP value and error at 95% confidence interval was measured to be (82.6 ± 0.2) $mV_{Ag/AgCl}$. All potentials are presented versus the saturated Ag/AgCl reference. The Cu/Al alloy couple was connected as the working electrode.

Journal Pre-proof

All regions of interest were also investigated in an argon environment to observe the effect of gaseous oxygen on the spreading of the droplet. A transparent chamber, as seen in Figure 2D, was fabricated with plastic and an opening to enable the entrance of the droplet and needle. The chamber was first filled with argon for 2 min before starting WCA experiments and PDP measurements. All measurements on each region and in both environments were replicated at least 3 times and average values and associated errors at 95% confidence are reported. The argon gas used was dry and the use of a water bath to control the H.R was not implemented in this work. However, all measurements were performed within ~30s of droplet/surface contact, where the amount of solvent evaporation within this time frame is small (10s of nLs) and should have minimal effect on the measured WCA.[24]

The experiments outlined were performed on one single sample within an afternoon, where the sample was not moved throughout the experiment to avoid misalignment with the dispensing/dosing heights.

2.4. Electrochemical Measurements and Coupling of Instruments

The Al alloy/Cu couple was placed on the goniometer stage and the dosing/deposit heights were set by performing WCA measurements over the surrounding resin. All needle heights then remained constant for all measurements. Once the OCP measurement commenced, the droplet was automatically approached using the predefined deposit height to the substrate, forming an electrical connection between the two electrodes. OCP was measured for 10s before automatically starting PDP measurements. This methodology was systematically used for each measured area. The scan rate was 100

Journal Pre-proof

mV/s. The OCP and scan rate were chosen to ensure the completion of the measurement before significant evaporation of the droplet, within the first minute of contact. All PDPs were initiated at -300 mV *vs.* OCP prior to the scan, and were completed at (1.082) $V_{Ag/AgCl}$ to collect both the cathodic and anodic Tafel branches. Once the measurement finished, the needle was retracted back to the dosing height and the droplet was allowed to evaporate in air to mark the analysed surface area. The sample was moved using the manual x and y positioners on the goniometer to the next region. All areas of interest were measured at least 3 times at different points along the surface and the average value and associated errors at 95% confidence are reported.

The placement of the needle at the interface was performed by eye. Due to the approximate placement and the shape of the galvanic couple, the ratio of Al alloy to Cu was not well defined nor well controlled throughout this study, but can be measured after each experiment.

2.5. Microscopy and Surface Analysis

Once all droplets had evaporated, the footprint from the droplet was observed using an optical microscope and images at 5x the magnification were captured. The surface areas were measured using ImageJ software (V. 1.48) using either the circle tool or by free hand to draw a perimeter around the corroded areas. These values were used to normalize the corresponding PDP measurements. Average grain sizes were estimated using the line intercept method.

Journal Pre-proof

Scanning electron microscopy (SEM) images in secondary electron mode were obtained to observe the microstructure of the corrosion products formed on Cu using a ZEISS Ultra 55 microscope. The chemical composition of corrosion products was investigated using energy dispersive X-ray analysis (EDX). The EDX corrosion product analysis was rationalized via simulation using Hydra/Medusa software to model the thermodynamically stable corrosion products expected to be present at the estimated pH and chloride concentration of the electrolyte.

3. Results and Discussion

3.1. Wettability of Metals

The static WCAs were measured on each area of interest (Al alloy, Cu, interface). The wettability measurements were first carried out without the needle in contact with the droplet to confirm that the needle did not obstruct the WCA measurements. The average WCA value on the Al alloy was 76° ± 2, while Cu portrayed a WCA of 93° ± 1. The difference in values indicates a difference in surface energy between the two metal surfaces. The higher the WCA, the lower the surface energy of the material and the less it interacts with water. The WCA of Cu is over 90°, indicating that this substrate's surface portrays hydrophobic behaviour at this surface state and roughness. Such hydrophobicity could be present due to the metal's inherent lower surface energy due to the formation of a lower energy oxide film, and/or contamination of the Cu surface from volatile organic compounds in comparison to the level of contamination on the Al alloy.[25–27] In fact, there will always be some sort of surface layer on metals, which masks their true surface energy while in any other environment other than in vacuum. Nonetheless, it has been

Journal Pre-proof

previously documented that Cu portrays a higher WCA than Al,[28] reflecting similar results to what is reported here.

Although surface roughness can influence the intrinsic WCA measured, both metals were polished exactly in the same manner, i.e., at the same time since they were physically coupled, so the influence of minor surface roughness differences or time to form an oxide film cannot solely explain the larger discrepancy in WCAs of the two substrates.

WCA values were extracted for a droplet residing at the interface of the two metals. The values measured on the Al alloy and Cu regions were 86° and 70°, respectively. The wettability on the Al alloy side is lower to what was observed solely on the alloy, while the wettability on the Cu side is higher than what was measured on pure Cu. An average for WCA measurements at the interface is not reported due to the geometry of the sample used and limited number of areas available for analysis within the single sample.

3.2. Open Circuit Potential Measurements

Electrical connections were first established between the goniometer needle and the metal substrate in order to measure OCP values. Examples of the electrochemical response for each area (pure Cu, Al alloy, and interface) can be seen in Figure 3. First, the 0.05 M NaCl droplet was dispensed while the needle was far from the substrate at the set dosing height, and the OCP measurement was started (region 1 in Figure 3A and B). As the droplet approached and wetted the surface at a rate of ~0.5 mm/s, a potential change was measured (region 2 in Figure 3A and B). Once the goniometer needle reached the final deposit height, the droplet was in complete contact with the substrate and corresponding

Journal Pre-proof

WCA and OCP values were obtained. The OCPs were stable for the ~8s measurement after the needle had halted at the deposit height for all areas analyzed, indicating that the metal reached steady state and validated the short timescale chosen to avoid evaporation.

The average OCP value measured on the Al alloy was (–0.801 ± 0.088) $V_{Ag/AgCl}$. The variability is due to the influence of intermetallic precipitates[29] present within the small area formed by the 0.4 μL droplet. The metallurgy of Al alloys has been extensively studied,[30] where alloying elements can precipitate from the metal matrix to form intermetallic regions that possess different electrochemical reactivity than the surrounding Al matrix and can alter the mixed potential measured.[12] Such precipitates can also potentially influence the uniformity and stability of the formed oxide film. The pure Cu regions portray a more noble OCP, of about (0.212 ± 0.022) $V_{Ag/AgCl}$. Copper is known for its corrosion resistance, as it is noble on the electromotive series, thus it possesses a higher OCP with respect to the Al alloy. The variability is also much lower than the Al alloy due to the metal's uniform microstructure (i.e., less inclusions/precipitates than an alloy), thus a more uniform and stable oxide film could form. The variability measured on metallic Cu could be due to impurities present from manufacturing processes. Lastly, the average OCP value measured at the interface of the galvanic couple was (–0.395 ± 0.041) $V_{Ag/AgCl}$ and is between the values obtained on the individual metals. This is in agreement with the mixed potential theory, where the OCP value of two metals in electrical contact is located between the OCP of the two metals measured separately.

Journal Pre-proof

3.3. Voltammetry in Aerated Droplet

Once OCP measurements were completed, potentiodynamic polarization (PDP) was initiated -300 mV below OCP to obtain the cathodic Tafel branch. Examples of voltammetry measurements on each metal and at the interface are presented as Tafel plots in Figure 4A. Images of the droplets at time of deposition (designated t = 0s) and after the PDP measurements are presented in Figure 4B-D. The WCA values on each metal measured right after deposition are not statistically different than the measurements performed without the needle in contact with the droplet for the Al alloy and Cu areas. The WCAs on the interface region at t = 0s are different than measurements without the needle, however, which could be due to the different ratios of metal coverage under the droplet at each region, and/or due to the angle at which the droplet was positioned with respect to the camera.

Average corrosion parameters were extracted from the PDP measurements and can be found in Table 1. All corrosion potentials, E_{corr}, are lower than the OCP values measured prior to measurements. This is due to the cathodic potential applied to the substrate 300 mV lower than the OCP. Oxidizing agents present (O_2, metal ions) are reduced on the metal surface and can change the local pH chemistry. Both Al and Cu form oxide/hydroxide films while immersed in aqueous electrolytes. These films could be destabilized by the local pH changes, thus thinning the protective passive film and lowering E_{corr}. Breakdown potentials observed on the anodic Tafel branch of the PDP measurements indicate that the passive films were compromised. Cu showed a breakdown potential of 0.4 $V_{Ag/AgCl}$. The Al alloy and interface PDP curves show

Journal Pre-proof

similarities in the shape and magnitudes of their second passive regions from 0.2 to 0.75 $V_{Ag/AgCl}$. The Al alloy showed a small peak around -0.1 $V_{Ag/AgCl}$, which is unique to this metal, as the interface did not portray such behavior. This confirms that this peak is not due to the QRCE steel needle, but is an electrochemical response measured on the Al alloy, possibly due to the intermetallic precipitates present.

Table 1. average values and associated errors at 95% confidence of corrosion parameters E_{corr} and j_{corr} extracted from PDP measurements performed in air of Al alloy, pure Cu, and at the interface.

Corrosion Parameter	Al alloy	Interface	Cu
E_{corr} ($V_{Ag/AgCl}$)	-0.934 ± 0.074	-0.525 ± 0.057	0.104 ± 0.031
j_{corr} (μA/mm^2)	0.088 ± 0.014	0.139 ± 0.004	0.089 ± 0.018

Average corrosion current densities, j_{corr}, were extracted by extrapolating the intersection of the linear regions of the cathodic and anodic Tafel branches for each PDP measurement. The corrosion rates for the pure Cu and Al alloy are similar, with values of 0.089 ± 0.018 μA/mm^2 and 0.088 ± 0.014 μA/mm^2, respectively. The cathodic reaction on Al alloy is hydrogen evolution, which was confirmed by the formation of bubbles during anodic polarization. The cathodic reaction on Cu is oxygen reduction, where no bubble formation occurred. The interface demonstrated a higher j_{corr} of 0.139 ± 0.004 μA/mm^2. This is due to the galvanic coupling of the two metals, where the more active metal, in this case Al alloy, acts as the anode:

$$Al_{(s)} \rightarrow Al^{3+}_{(aq)} + 3e^- \quad (1)$$

While the more noble metal, Cu, enables the reduction of oxygen at neutral pH (~6.5-7):

$$O_{2(g)} + 2H_2O_{(l)} + 4e^- \rightarrow 4OH^-_{(aq)} \quad (2)$$

The electrical contact between the two metals accelerates the electrochemical oxidation of the Al alloy, increasing the current density while reduction of oxygen occurring on Cu balances the electrochemical reaction.

3.4. Wettability and Surface Area after PDP Measurements

After PDP measurements, WCA values were extracted to monitor the change in wettability due to polarization, as seen in Figure 4B-D. It was hypothesized that a change in surface energy (WCA) due to applied polarization could be observed via the combination of instruments utilized here. The wettability of Cu did not change during polarization. This could be attributed to the precipitation of insoluble species formed on Cu during air exposure (Cu oxides) that acted as a protective barrier, where no active metal was exposed to increase the overall wettability. This also suggests that any potential newly formed surface species due to electrochemical polarization did not influence the metal's apparent wettability. Nonetheless, the effect of surface preparation and chemistry will be studied in future work. Furthermore, as seen in the PDP response of Cu, a transpassive potential was not observed, indicating that the metal's surface film was not detrimentally compromised within the potential window analyzed, and therefore continued to inhibit wettability changes.

A significant decrease in WCA value on Al alloy, however, was measured, where the value decreased 8° after PDP. During polarization, the Al alloy's protective surface film (passive film) is compromised, which is signified by the transpassive potential present in the PDP response. Thus, it can be hypothesized that this phenomenon exposes active

Journal Pre-proof

metal available for oxidation/repassivation, thus increasing the overall wettability (surface energy) of the analyzed surface. Other hypotheses to account for such increase in wettability include a change in passive film chemistry composed of hydroxides, an increase in surface roughness, and/or because of adsorbed hydrogen on the surface. However, in this work, the droplet size is large in comparison to the droplet size used in advanced EDC methods, which causes a loss in WCA resolution to observe localized (re)passivation events that affect changes in surface energy. Miniaturization of the droplet, as well as the investigation of other metals, is planned for future work in order to expand on this phenomenon.

It is realized that although WCA is related to surface energy, this parameter is difficult to interpret in terms of energy due to the convoluted effects of geometry (surface roughness and droplet shape) and dynamic surface chemistry. However, if the assumption is made that the geometries of the drop and surface are ideal and that there is no change in surface chemistry, an estimation of the adhesion work between the solid surface and the liquid can be calculated, which is linked to the energy released by the wetting phenomenon.

Applying the Young equation:

$$\gamma^{LV}\cos\theta = \gamma^{SV} - \gamma^{SL} \quad (3)$$

where γ^{LV} is the liquid-vapour surface tension, γ^{SV} is the solid-vapour surface tension, γ^{SL} is the solid-liquid surface tension, and θ is the inherent contact angle at the triple phase point, the value of γ^{SL} can be evaluated from variation in θ. Assuming that γ^{SV} is constant and at equilibrium, and γ^{LV} is a known value of 72.8 mN/m for water-air interface at room temperature, the variation of the contact angle is directly related to the

changes at the solid and liquid interface. In the case for the Al alloy evaluated here, the change in wetting would account for an increase of 10 mN/m after polarization. However, we present a real system where changes in droplet geometry and surface chemistry can be significant. Nonetheless, the direct WCA measurement provides us a good estimate of the interaction between the liquid and the substrate.

Measurements performed at the interface presented a significant change in WCA on both the Al alloy and Cu regions. The WCA value decreased 8° over the Al alloy, the same amount as what was measured solely on the metal. On the Cu region, however, the WCA decreased 15° over the course of a PDP measurement. This sudden increase in wettability on Cu increased the wetted surface area, where the droplet edge on the Cu side shifted throughout the measurement.

The resulting footprints created by salt crystallization and corrosion product after the electrochemical measurements were measured to obtain the true surface area of the region analyzed. By marking each measurement's location, the corresponding PDP curve was normalized by the true surface area rather than estimated via the pipette aperture. This approach enables the extraction of a more accurate current density. Footprints obtained at OCP while leaving the needle in contact with the droplet for the same amount of time as the electrochemical experiments were also analyzed to compare morphology, size, and composition to that of an area that underwent PDP. In Figure 5, examples of resulting footprints from OCP measurements on all regions of interest can be seen in the top row (A-C), while footprints due to PDP are presented in the bottom row (D-F).

Journal Pre-proof

At OCP, the footprint on the Al alloy does not demonstrate a strong change in colour, but is outlined by a perimeter of NaCl crystals formed during droplet evaporation, as seen in Figure 5A. Under polarization, however, discolouration within the footprint is observed due to the formation of Al rich hydroxides/chlorides, and the grain structure and size (diameter of 160 ± 15 μm) is revealed (Figure 5D). Different crystallographic orientations possess different reactivity, which can impact the wettability (surface energy) of the metal.[10,31–33] This observation confirms that the droplet size is much larger than the grain size (at least 7x larger), and therefore we obtained an averaged response of different grain orientations. As seen in Table 2, the average surface area at OCP was smaller than what was measured after PDP measurements. This result is in agreement with the decrease of WCA values obtained before and after PDP, where the increase in surface area is due to changes in surface energy from the applied potential.

In comparison, corrosion can be seen within the footprint formed at OCP over the pure Cu in Figure 5B, as corrosion products are observed by the signature blue/green coloured Cu (II) hydroxide species that have been extensively characterized previously via chemical analysis.[34] However, the colour change is much more apparent within footprints of polarized areas, where Cu (II) hydroxide/chloride (blue/green in colour) is present within the exposed grain boundaries and darker Cu (I) species are observed on the grain faces.[35] The average surface areas for both cases are not statistically different. This is also in agreement with the WCA measurements obtained using the goniometer before/after PDP measurements.

Journal Pre-proof

The measured surface areas over interface regions are the most interesting. Even at OCP, as seen in Figure 5C, a large crevice was formed on the Al alloy at the interface between the two metals. The crevice increased the surface area and roughness of the analyzed surface, yet the change in WCA values extracted over the Al alloy did not change from what was observed solely on the metal alloy. This lowers the probability that the change in surface roughness induced by corrosion is responsible for the drop in WCA values, but is more likely to be caused by changes in surface chemistry. Furthermore, the wetted surface area was dynamic. Droplet spreading on the Cu region can be observed, where initially the droplet was smaller; a similar size to what was observed on Al alloy, then grew over time. These features were also observed on the polarized regions (Figure 5F). The growth of the droplet rather than contraction was confirmed by the images taken with the goniometer camera in Figure 4D, as well as the smaller amount of Cu hydroxides present (observed via smaller regions covered by blue/green corrosion product) within the exterior footprint, indicating the precipitates had less time to grow.

Droplet spreading only affected the Cu region within the interface area, whereas the wetted area remained constant on the Al alloy. This phenomenon was hypothesized to be due to diffusion of oxygen from the surrounding environment at the droplet edges, a region of high surface tension, which causes the growth of hydroxide corrosion product at this region. To validate this hypothesis, experiments were conducted under an anaerobic environment, as presented in the following sections.

Journal Pre-proof

The surface areas of the interior footprint, i.e., when the droplet is initially in contact with the substrate (t = 0 s), and of the exterior footprint, i.e., at the end of the experiments (after PDP) can be seen in Table 2. The interior footprint is larger than values extracted for both the Cu and Al alloy due to the galvanic coupling of the materials. The exterior footprints are significantly larger than the interior values, which induce an error of (18 ± 2)% and (17 ± 1)% in the surface area at OCP and during PDP, respectively.

The change in surface area throughout OCP and PDP measurements is of great importance when extracting corrosion parameters at the microscale. This infers that the surface area is dynamic and the changing surface area as a function of time must be used to normalize each data point measured during electrochemical measurements in order to obtain an accurate value and estimation of corrosion rate. In this study, however, the exterior footprint surface areas were used to normalize the PDP measured at the interface regions. This is because the wetted area is not well defined due to the surface roughness induced by grinding/polishing, as well as the large crevice formed at the interface of the two metals. Crevices impose a higher surface area than what is measured from the 2D images of the footprints and should be measured using a topographical technique, i.e., atomic force microscopy or profilometry. Nonetheless, this is a good first estimate in comparison to estimating the surface area by the needle aperture.

Poor estimation of the working electrode surface area during micro droplet experiments would result in underestimating the measured j_{corr}. In advanced EDC methods SECCM/SMCM, the surface area of the working electrode is often assumed to be the

Journal Pre-proof

aperture diameter of the capillary used in the experimental setup. The inner diameter of the capillary is taken for this assumption due to the relation found by Lippmann, which showed that the size of a mercury droplet was related to the inner diameter of the capillary.[36] The inner diameter of the syringe needle was 275 µm. If used to estimate the surface area of the working electrode, all droplet footprints would be 0.059 mm^2, a value that is two orders of magnitude smaller than the true values measured *ex situ*. Alternatively, the working electrode surface area could be calculated by the droplet volume of 0.4 µL. This scenario imposes the assumption of ideal droplet geometry, and results in an estimated value of 0.003 mm^2, even smaller than the estimated value using the needle aperture, and therefore proves this assumption to be insufficient. This is of importance while performing SECCM/SMCM corrosion measurements without a silicon skirt, where droplet surface area (working electrode surface area) is currently routinely estimated by the size of the pipette aperture. In order to further the understanding of corrosion initiation mechanisms on the nano/micro scale, the need for accurate and reliable experimental data is crucial.

Journal Pre-proof

Table 2: average surface areas obtained from measuring each footprint and the associated errors at 95% confidence in air.

Surface area (mm^2)	Al alloy	Cu	Interface (t = 0s)	Interface after PDP
30s OCP	1.03 ± 0.04	1.23 ± 0.03	1.37 ± 0.04	1.67 ± 0.06
OCP + PDP	1.26 ± 0.09	1.21 ± 0.11	1.46 ± 0.07	1.75 0.07

3.5. Experiments under Anaerobic Conditions

The electrochemical/surface energy experiments were performed in the same fashion as the measurements done in air. A transparent chamber was used to isolate the experimental area and a flow of argon replaced the air inside to create an anaerobic environment. During measurements, the flow of argon was stopped in order to avoid deformation of the drying droplets to ensure that the footprints formed were accurate representations of the surface area analyzed.

The OCP values measured on Al alloy, Cu, and the interface were (–0.971 ± 0.119) V, (0.219 ± 0.062) V, and (–0.316 ± 0.030) V all vs. sat. Ag/AgCl, respectively. These values are not statistically different to what was measured in air. After 8s of OCP to make electrical contact with the substrate, PDP measurements were carried out and example plots can be seen in Figure 6A.

The voltammetry under argon resembles the same behavior as obtained in an aerated environment, where average corrosion parameters can be found in Table 3. E_{corr} values for Cu and Al alloy are not statistically different, and j_{corr} values vary only slightly. This is because the electrolyte was not purged of oxygen; hence the cathodic reaction can be carried out to ensure that only the oxygen available in the droplet participates to the cathodic reaction. The E_{corr} value at the interface was more noble than in air, however, where such variation can be due to the difference in metal ratios examined. It has been previously shown on polycrystalline Zn that current densities measured in argon are much smaller than values measured in air.[14] However, all data in this study was

Journal Pre-proof

normalized by the pipette aperture opening rather than the true wetted surface area formed under the droplet. Here, we normalize by the droplet footprint surface area, which shows that the current densities in air and in argon are similar for the metals investigated.

Table 3: average values and associated errors at 95% confidence of corrosion parameters E_{corr} and j_{corr} extracted from PDP measurements performed in argon of Al alloy, pure Cu, and at the interface.

Corrosion Parameter	Al alloy	Interface	Cu
E_{corr} ($V_{Ag/AgCl}$)	-1.05 ± 0.102	-0.424 ± 0.015	0.132 ± 0.053
j_{corr} (μA/mm^2)	0.066 ± 0.012	0.126 ± 0.056	0.088 ± 0.018

Images and corresponding WCAs taken at t = 0s and after PDP measurements for each region of interest can be seen in Figure 6 B-D. WCA values are similar to what was measured previously in air; the wetting on Cu remains constant throughout PDP measurements and the wettability of Al alloy increases with during PDP measurements, where the WCA decreases by 7°. Therefore, the same wetting mechanism can be hypothesized to occur in argon as in air on the pure metals. WCA values at the interface follow the same trend as seen in air, although values differ slightly due to the positioning of the droplet and the angle of the camera. The values on both metals change during polarization, yet the droplet size did not vary. This may be due to slightly different evaporation rates of the droplets throughout measurements in the dry argon environment.

Footprints from OCP and PDP measurements can be seen in Figure 7, where the top row (A-C) were obtained after OCP, whereas the bottom row (D-F) were taken after PDP. The droplet size, or surface area, was measured for both experiments and tabulated values

can be found in Table 4. All corresponding PDP plots were normalized by the surface area measured in the optical images.

Table 4. average surface areas obtained from measuring each footprint and the associated errors at 95% confidence in argon.

Surface area (mm^2)	Al alloy	Cu	Interface (after PDP)
30s OCP	1.49 ± 0.12	1.31 ± 0.17	--
OCP + PDP	1.42 ± 0.03	1.51 ± 0.06	1.86 ± 0.06

The footprints on Al alloy at OCP present a different salt crystallization pattern, where concentric rings are observed within the wetted area. The colour inside the droplet footprint is similar after polarization, indicating that the metal is not corroding during PDP as severely as it did in air. Furthermore, the corrosion pattern is different, where the grain boundaries are not visible after PDP.

As for Cu, at OCP, some regions within the footprint appear intact after contact. After PDP, however, discolouration due to corrosion product formation is observed. The colouring is much darker and different than what was seen in air, where very little green/blue Cu (II) hydroxide corrosion product is observed. The grain boundaries are also not exposed after PDP as they were in air. This may indicate a different corrosion mechanism occurring in deaerated environments as opposed to in air.

Measurements performed at the interface show different behavior than in air. At OCP, areas within the Cu region are intact, similar to observations on the pure Cu. The

Journal Pre-proof

perimeter of the footprint is very well defined, unlike in air. There is no exterior droplet footprint, nor does a crevice initiate at the interface of the dissimilar metals. Similar results are observed during PDP measurements. Although the humidity within the argon environment is lower than in air, the surface being analyzed cannot be dried within the short timeframe of the argon purge (2 min). Since an air-formed oxide film covers the metal surfaces, which is very hygroscopic, and the measurement timescale is short, it's impossible to completely dry the surface to affect the droplet spreading behavior. This validates the hypothesis that droplet spreading occurs due to oxygen diffusion at the droplet edges, whereas in argon, only oxygen within the aerated electrolyte is available for the cathodic reaction on Cu. This also means that the crevice formed on the Al alloy at the interface in air is driven by this phenomenon.

The results presented are important for two reasons. Firstly, this work sheds light on the importance of intermetallic regions on localized corrosion during atmospheric corrosion. If a droplet of liquid condenses onto a region including an interface, the diffusion of oxygen at the edges of the droplet on the more noble metal will accelerate the oxidation of the active metal, causing a localized corrosion mechanism and self-perpetuating degradation. Secondly, conducting experiments under a blanket of argon can minimize dynamic wetting during EDC measurements. This eliminates the need for a silicon gasket and the potential of crevice corrosion to form under this barrier. The voltammetry is similar to the response in air due to the reservoir of oxygen within the electrolyte, but this environment inhibits the spreading of the droplet, thus data does not need to be

Journal Pre-proof

normalized by a surface area time dependence function, but simply by the footprint of the droplet measured *ex situ.*

To investigate the morphology and composition of corrosion product within the spreading region, SEM/EDX analysis was carried out in the following section.

3.6. Analyzing Corrosion Product and Validating Corrosion Mechanism

After polarization at the interface in air, the droplet was allowed to dry and the area's chemical composition was investigated. A secondary electron SEM image of the footprint can be found in Figure 8A along with EDX mapping of Cu, Cl, and O. Figure 8B shows a schematic of the proposed corrosion mechanism and the corrosion products formed at pH~6 from thermodynamic prediction of species.

The crevice formed close to the interface of the two metals is observed on the Al alloy as a shallow, moat-like crater ~200 μm in thickness and spans the entire diameter of the wetted area. Corrosion product and salt deposit surrounds this region due to the local changes in pH inside the crevice. Corrosion product is also present on the Cu region, as seen as darker areas in Figure 8A. A small area was analyzed for its chemical composition to reveal the formation of a dendritic patterned material with high content of Cl and Cu. Surrounding the $CuCl_2$ dendrites was corrosion product with a high content of oxygen. The experimental findings of the corrosion product composition are in agreement with what was predicted via the Hydra/Medusa simulation.

Journal Pre-proof

On pure metals, the cathodic reaction on Al alloy is hydrogen evolution,[37] while oxygen reduction balances the oxidation of Cu. When galvanically coupled, however, oxygen reduction can occur on the cathodic Cu region, while the Al alloy is sacrificed as the anode and corrodes. If the droplet is surrounded by air, gaseous oxygen diffuses into the droplet at the edges, where it is consumed to form hydroxide that reacts with chemically dissolved Cu and the oxidized Al species to form $Cu(OH)_2$ and $Al(OH)_3$, respectively. The formation of hydroxides and the change in surface energy at the droplet edge on Cu increases the wettability. The coupled Al enables a large current density to flow, and the protective passive film at the edge of the Cu becomes compromised.

Droplet corrosion chemistry is not a novel concept- Evans in 1926 investigated the local pH changes within a droplet on polycrystalline Fe using chemical indicators. The edges of the droplet turned pink (via phenolphthalein) due to the highly alkaline environment that formed from an increase in hydroxide concentration on the cathodic region. The interior of the droplet turned blue (via potassium ferricyanide) as the region became anodic and localized corrosion was observed.[38] This phenomenon was attributed to the distribution of oxygen and the high surface tension at the edges of the droplet, where Evans later proposed a device to equally expose metal surfaces to dissolved oxygen in order to avoid the production of a deaerated anodic area vulnerable to localized attack.[39] A similar mechanism is proposed in the current work, however, due to the galvanic coupling of Al alloy and Cu, the anodic reaction is supported at the more active metal in contact with the cathodic metal.

Journal Pre-proof

The analysis of galvanic corrosion in an equilibrated droplet is of interest to the atmospheric corrosion community- corrosion that occurs inside small condensed droplets of liquid. Policastro et al. investigated the galvanic corrosion current between an Al alloy and stainless steel through experimental and theoretical predictions to further the understanding of atmospheric corrosion at the interface of the metal system.[40] However, the two metals were not physically in contact with one another, but an insulating resin isolated them from one another so the galvanic corrosion current could be measured. Although authors concluded that the corrosion mechanism relied on the blocking of ion transport due to electrolyte chemical reactions to minimize further degradation,[40] the experimental setup lacks a depth of real in-use configuration. While in-use, dissimilar metals are often in physical contact with one another, and the local interfacial electrochemical and chemical changes that occur are critical in dictating corrosion mechanisms. Furthermore, such studies do not capture the changes and effect of wetting and hence surface energy changes on the two dissimilar metals. This highlights the potential for the combined setup used in this work to further enhance the corrosion community's knowledge about interfacial corrosion chemistry inside of droplets.

Journal Pre-proof

4. Conclusions

The combination of a goniometer and potentiostat has enabled the observation of changes in surface energy/ wettability during micro electrochemical measurements. The results at the length scale presented show that polarization of a metal surface can impact its surface energy, but are dependent on the metal's interfacial stability under the experimental conditions used. Wetting at the interface of two metals creates a galvanic couple, which accelerates the corrosion of the active metal and enables the noble metal to undergo

cathodic protection. In air, oxygen diffuses at the edges of the droplet where the surface tension is high, causing heterogeneous spreading on the cathodic metal as a function of time. This study underlines the difficulty of downscaling corrosion science, particularly when EDC systems are used. When extracting corrosion current density, the surface area cannot be estimated by the pipette aperture as this creates an over estimated corrosion rate on the micro/nano scale. Either normalization by the true surface area as a function of time due to spreading can be performed, or the use of an anaerobic environment can help limit droplet spreading to accurately extract the analyzed surface area. Electrolyte, droplet size and surface preparation/composition will be explored and considered in future experiments.

Author Contributions

S.M.G conceptualized experimental setup and application, performed data analysis, and prepared the manuscript draft. S.M.G and O.G conceptualized and performed experiments, and organized data/figures. All authors contributed to data interpretation, discussion, and editing.

Declaration of interests

The authors declare that they have no known competing financial interests or personal relationships that could have appeared to influence the work reported in this paper.

Acknowledgements

S.M.G gratefully acknowledges the Natural Sciences and Engineering Research Council of Canada (NSERC) for her PDF NSERC scholarship. O.G is grateful for the L'Oréal-

Journal Pre-proof

UNESCO fellowship for Women in Science Fellowship. Authors thank Stephanie Delbrel for acquiring the SEM images.

References

[1] H. Böhni, T. Suter, A. Schreyer, Micro- and nanotechniques to study localized corrosion, Electrochim. Acta. 40 (1995) 1361–1368. https://doi.org/https://doi.org/10.1016/0013-4686(95)00072-M.

[2] T. Suter, H. Böhni, A new microelectrochemical method to study pit initiation on stainless steels, Electrochim. Acta. 42 (1997) 3275–3280. https://doi.org/10.1016/S0013-4686(70)01783-8.

[3] R.A. Perren, T. Suter, C. Solenthaler, G. Gullo, P.J. Uggowitzer, H. Böhni, M.O. Speidel, Corrosion resistance of super duplex stainless steels in chloride ion containing environments: investigations by means of a new microelectrochemical method: II. Influence of precipitates, Corros. Sci. 43 (2001) 727–745. https://doi.org/https://doi.org/10.1016/S0010-938X(00)00088-3.

[4] M.M. Lohrengel, A. Moehring, M. Pilaski, Capillary-based droplet cells: limits and new aspects, Electrochim. Acta. 47 (2001) 137–141. https://doi.org/https://doi.org/10.1016/S0013-4686(01)00570-9.

[5] M.M. Lohrengel, C. Rosenkranz, I. Klüppel, A. Moehring, H. Bettermann, B.V. den Bossche, J. Deconinck, A new microcell or microreactor for material surface investigations at large current densities, Electrochim. Acta. 49 (2004) 2863–2870. https://doi.org/https://doi.org/10.1016/j.electacta.2004.01.068.

[6] R. Oltra, B. Vuillemin, F. Thebault, F. Rechou, Effect of the surrounding aeration

Journal Pre-proof

on microcapillary electrochemical cell experiments, Electrochem. Commun. 10 (2008) 848–850. https://doi.org/https://doi.org/10.1016/j.elecom.2008.03.014.

[7] N. Birbilis, B.N. Padgett, R.G. Buchheit, Limitations in microelectrochemical capillary cell testing and transformation of electrochemical transients for acquisition of microcell impedance data, Electrochim. Acta. 50 (2005) 3536–3544. https://doi.org/https://doi.org/10.1016/j.electacta.2005.01.010.

[8] C.L. Bentley, M. Kang, P.R. Unwin, Scanning electrochemical cell microscopy: New perspectives on electrode processes in action, Curr. Opin. Electrochem. 6 (2017) 23–30. https://doi.org/https://doi.org/10.1016/j.coelec.2017.06.011.

[9] L.C. Yule, V. Shkirskiy, J. Aarons, G. West, C.L. Bentley, B.A. Shollock, P.R. Unwin, Nanoscale Active Sites for the Hydrogen Evolution Reaction on Low Carbon Steel, J. Phys. Chem. C. 123 (2019) 24146–24155. https://doi.org/10.1021/acs.jpcc.9b07216.

[10] L.C. Yule, V. Shkirskiy, J. Aarons, G. West, B.A. Shollock, C.L. Bentley, P.R. Unwin, Nanoscale electrochemical visualization of grain-dependent anodic iron dissolution from low carbon steel, Electrochim. Acta. 332 (2020) 135267. https://doi.org/https://doi.org/10.1016/j.electacta.2019.135267.

[11] P. Letellier, A. Mayaffre, M. Turmine, On the solvent evaporation for a sessile drop: Solvent–vapour equilibrium must be achieved in open system, Colloids Surfaces A Physicochem. Eng. Asp. 355 (2010) 197–200. https://doi.org/https://doi.org/10.1016/j.colsurfa.2009.11.043.

[12] Y. Li, A. Morel, D. Gallant, J. Mauzeroll, Oil-Immersed Scanning Micropipette Contact Method Enabling Long-term Corrosion Mapping, Anal. Chem. 92 (2020)

Journal Pre-proof

12415–12422. https://doi.org/10.1021/acs.analchem.0c02177.

[13] Y. Li, A. Morel, D. Gallant, J. Mauzeroll, Ag+ Interference from Ag/AgCl Wire Quasi-Reference Counter Electrode Inducing Corrosion Potential Shift in an Oil-Immersed Scanning Micropipette Contact Method Measurement, Anal. Chem. (2021). https://doi.org/10.1021/acs.analchem.1c01045.

[14] V. Shkirskiy, L.C. Yule, E. Daviddi, C.L. Bentley, J. Aarons, G. West, P.R. Unwin, Nanoscale Scanning Electrochemical Cell Microscopy and Correlative Surface Structural Analysis to Map Anodic and Cathodic Reactions on Polycrystalline Zn in Acid Media, J. Electrochem. Soc. 167 (2020) 41507. https://doi.org/10.1149/1945-7111/ab739d.

[15] C. Molena de Assis, T.H. Ho, H.G. de Melo, M. Keddam, M. Turmine, V. Vivier, Electrochemical Impedance Spectroscopy in a Droplet of Solution for the Investigation of Liquid/Solid Interface, Anal. Chem. 88 (2016) 12108–12115. https://doi.org/10.1021/acs.analchem.6b02795.

[16] S.M. Gateman, I. Halimi, A.R. Costa Nascimento, R. Lacasse, R. Schulz, C. Moreau, R. Chromik, J. Mauzeroll, Using macro and micro electrochemical methods to understand the corrosion behavior of stainless steel thermal spray coatings, Npj Mater. Degrad. 3 (2019) 25. https://doi.org/10.1038/s41529-019-0087-0.

[17] L.C. Yule, E. Daviddi, G. West, C.L. Bentley, P.R. Unwin, Surface microstructural controls on electrochemical hydrogen absorption at polycrystalline palladium, J. Electroanal. Chem. 872 (2020) 114047. https://doi.org/https://doi.org/10.1016/j.jelechem.2020.114047.

Journal Pre-proof

[18] S.M. Gateman, N.S. Georgescu, M.-K. Kim, I.-H. Jung, J. Mauzeroll, Efficient Measurement of the Influence of Chemical Composition on Corrosion: Analysis of an Mg-Al Diffusion Couple Using Scanning Micropipette Contact Method, J. Electrochem. Soc. 166 (2019) C624–C630. https://doi.org/10.1149/2.0681916jes.

[19] N. Birbilis, B. Hinton, Corrosion and corrosion protection of aluminium, in: R.B.T.-F. of A.M. Lumley (Ed.), Fundam. Alum. Metall., Elsevier, 2011: pp. 574–604. https://doi.org/10.1533/9780857090256.2.574.

[20] N. Birbilis, R.G. Buchheit, Electrochemical Characteristics of Intermetallic Phases in Aluminum Alloys, J. Electrochem. Soc. 152 (2005) B140. https://doi.org/10.1149/1.1869984.

[21] J.-L. Wang, C. Ke, K. Pohl, N. Birbilis, X.-B. Chen, The Unexpected Role of Benzotriazole in Mitigating Magnesium Alloy Corrosion: A Nucleating Agent for Crystalline Nanostructured Magnesium Hydroxide Film, J. Electrochem. Soc. 162 (2015) C403–C411. https://doi.org/10.1149/2.0781508jes.

[22] O. Gharbi, S. Kumar Kairy, P.R. De Lima, D. Jiang, J. Nicklaus, N. Birbilis, Microstructure and corrosion evolution of additively manufactured aluminium alloy AA7075 as a function of ageing, Npj Mater. Degrad. 3 (2019) 40. https://doi.org/10.1038/s41529-019-0101-6.

[23] J. Ferrari, H.G. De Melo, N. Pébère, B. Tribollet, V. Vivier, Using LEIS to Evaluate Local Electrochemical Activity of Al 7475 T761/Cu Model Electrodes, ECS Meet. Abstr. (2012). https://doi.org/10.1149/ma2012-02/20/2133.

[24] S.K. Singh, S. Khandekar, D. Pratap, S.A. Ramakrishna, Wetting dynamics and evaporation of sessile droplets on nano-porous alumina surfaces, Colloids Surfaces

Journal Pre-proof

A Physicochem. Eng. Asp. 432 (2013) 71–81. https://doi.org/https://doi.org/10.1016/j.colsurfa.2013.04.070.

[25] S. Takeda, M. Fukawa, Y. Hayashi, K. Matsumoto, Surface OH group governing adsorption properties of metal oxide films, Thin Solid Films. 339 (1999) 220–224. https://doi.org/https://doi.org/10.1016/S0040-6090(98)01152-3.

[26] Z. Li, Y. Zheng, J. Zhao, L. Cui, Wettability of Atmospheric Plasma Sprayed Fe, Ni, Cr and Their Mixture Coatings, J. Therm. Spray Technol. 21 (2012) 255–262. https://doi.org/10.1007/s11666-011-9728-8.

[27] S.M. Gateman, K. Page, I. Halimi, A.R.C. Nascimento, S. Savoie, R. Schulz, C. Moreau, I.P. Parkin, J. Mauzeroll, Corrosion of One-Step Superhydrophobic Stainless-Steel Thermal Spray Coatings, ACS Appl. Mater. Interfaces. 12 (2020) 1523–1532. https://doi.org/10.1021/acsami.9b17836.

[28] D.J. Trevoy, H. Johnson, The Water Wettability of Metal Surfaces, J. Phys. Chem. 62 (1958) 833–837. https://doi.org/10.1021/j150565a016.

[29] N.Z. Khan, A.N. Siddiquee, Z.A. Khan, M. Ubaid, D. Bajaj, M. Atif, A. Khan, Microstructure evolution of Friction Stir Welded Dissimilar Aerospace Aluminium Alloys, IOP Conf. Ser. Mater. Sci. Eng. 404 (2018) 12002. https://doi.org/10.1088/1757-899x/404/1/012002.

[30] I. Polmear, D. StJohn, J.-F. Nie, M. Qian, Light Alloys: Metallurgy of the Light Metals, 5th ed., Elsevier, Oxford, 2017.

[31] A. Schreiber, J.W. Schultze, M.M. Lohrengel, F. Kármán, E. Kálmán, Grain dependent electrochemical investigations on pure iron in acetate buffer pH 6.0, Electrochim. Acta. 51 (2006) 2625–2630.

Journal Pre-proof

https://doi.org/https://doi.org/10.1016/j.electacta.2005.07.052.

[32] E. Martinez-Lombardia, Y. Gonzalez-Garcia, L. Lapeire, I. De Graeve, K. Verbeken, L. Kestens, J.M.C. Mol, H. Terryn, Scanning electrochemical microscopy to study the effect of crystallographic orientation on the electrochemical activity of pure copper, Electrochim. Acta. 116 (2014) 89–96. https://doi.org/10.1016/J.ELECTACTA.2013.11.048.

[33] K.A. Lill, A.W. Hassel, G. Frommeyer, M. Stratmann, Scanning droplet cell investigations on single grains of a FeAlCr light weight ferritic steel, Electrochim. Acta. 51 (2005) 978–983. https://doi.org/https://doi.org/10.1016/j.electacta.2005.05.068.

[34] J.P. Franey, M.E. Davis, Metallographic studies of the copper patina formed in the atmosphere, Corros. Sci. 27 (1987) 659–668. https://doi.org/https://doi.org/10.1016/0010-938X(87)90048-5.

[35] F. Arjmand, A. Adriaens, Influence of pH and Chloride Concentration on the Corrosion Behavior of Unalloyed Copper in NaCl Solution: A Comparative Study Between the Micro and Macro Scales, Materials (Basel). 5 (2012) 2439–2464. https://doi.org/10.3390/ma5122439.

[36] G. Lippmann, Relations entre les phenomenes electriques et capillaires, Ann. Chim. Phys. 5 (1875) 494–549.

[37] C. Laurent, F. Scenini, T. Monetta, F. Bellucci, M. Curioni, The contribution of hydrogen evolution processes during corrosion of aluminium and aluminium alloys investigated by potentiodynamic polarisation coupled with real-time hydrogen measurement, Npj Mater. Degrad. 1 (2017) 6. https://doi.org/10.1038/s41529-017-

Journal Pre-proof

0011-4.

[38] R.U. Evans, The Ferroxyl Indicator in Corrosion Research, Met. Ind. 29 (1926) 481.

[39] U.R. Evans, Oxygen Distribution as a Factor in Corrosion of Metals, Ind. Eng. Chem. 14 (1925) 363.

[40] S.A. Policastro, R.M. Anderson, C.M. Hangarter, Analysis of Galvanic Corrosion Current between an Aluminum Alloy and Stainless-Steel Exposed to an Equilibrated Droplet Electrolyte, J. Electrochem. Soc. 168 (2021) 041507. https://doi.org/10.1149/1945-7111/abf5a7.

Journal Pre-proof

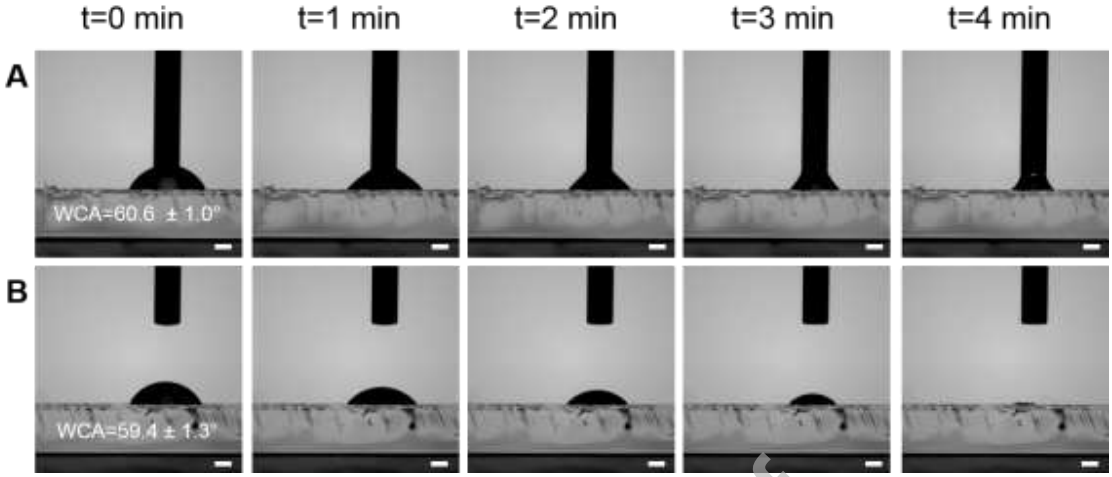

Figure 1: Monitoring droplet evaporation on glass A) with and B) without needle reservoir to estimate appropriate experimental timescale. The droplet size decreases until it is completely evaporated after 4 minutes when it is not in contact with the needle, while both the droplet size and shape change when the needle is present. Scale bar represents 500 μm.

Journal Pre-proof

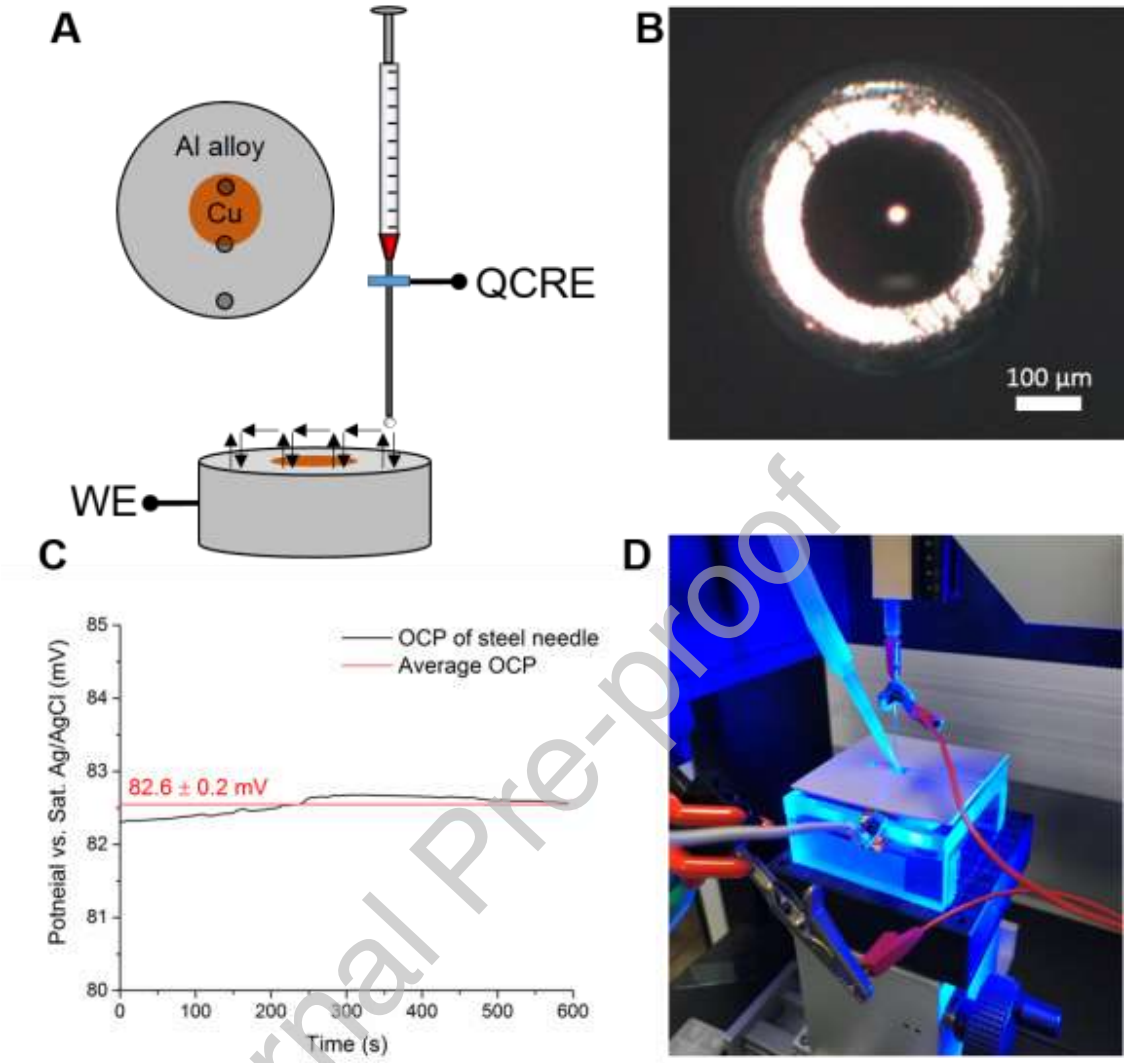

Figure 2: A) Schematic of the 2-electrode electrochemical setup used in this study, where the Cu/Al alloy served as the working electrode and the steel needle used to dispense the salt droplet acted as the quasi reference counter electrode. B) A front view micrograph of the steel needle aperture with an inner diameter of 274.7 µm. C) The potential difference of the steel needle and a commercial Ag/AgCl saturated reference electrode indicating a stable open circuit potential of the QRCE. D) A photograph of the experimental setup during measurements performed under argon.

Journal Pre-proof

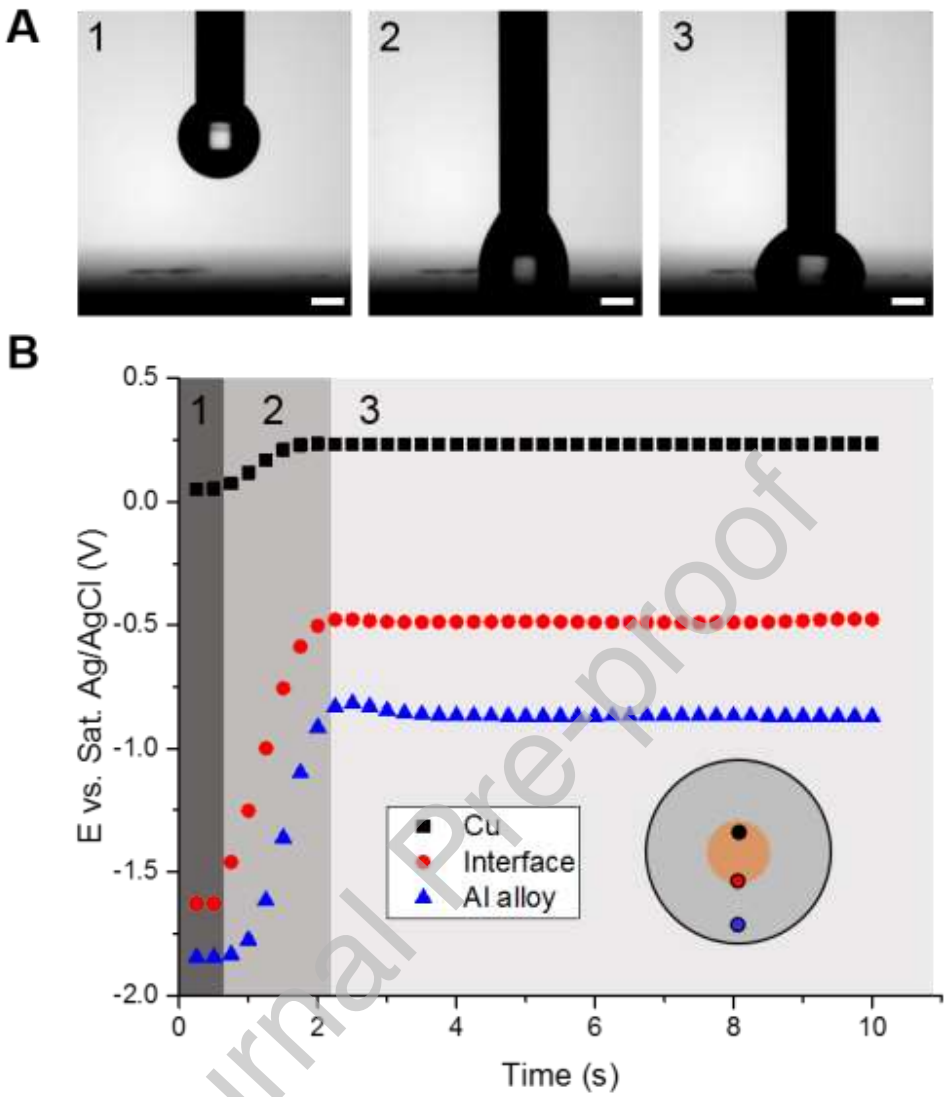

Figure 3: The methodology used to make electrical contact with the substrate. A) Shows snap shots taken during droplet deposition on Al alloy and B) demonstrates the electrochemical response of the OCP for each area approached. First, the 0.4 µL droplet of 0.05 M NaCl was created at the needle tip (1), followed by commencing the OCP measurement. Next, the droplet approached the substrate and made initial electrical contact, observed by the sudden change in OCP values (2). Finally, the droplet reached equilibrium with the air and metal surface interfaces, where stable OCP values were measured for ~8s before starting the potentiodynamic polarization scan. Scale bar represents 500 µm.

Journal Pre-proof

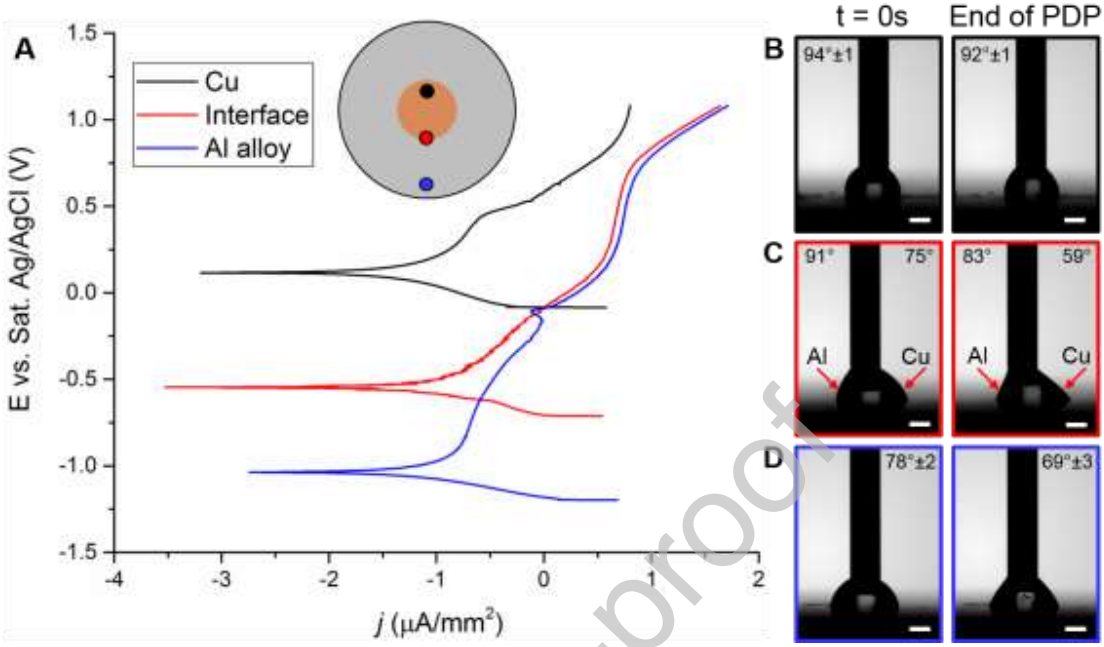

Figure 4: A) Representative potentiodynamic polarization curves obtained for each region investigated in an aerated environment: pure copper (black), Al alloy (blue), and at the interface of the two metals (red). A schematic is added to aid in the visualization of the sampled regions. B-D) Corresponding optical images of the 0.05 M NaCl droplets taken using the goniometer system before and after PDP measurements. The droplet is symmetrical on the B) Al alloy and D) Cu surfaces throughout the measurement, while the water contact angle is asymmetrical at the interface. Scale bars represent 500 μm.

Journal Pre-proof

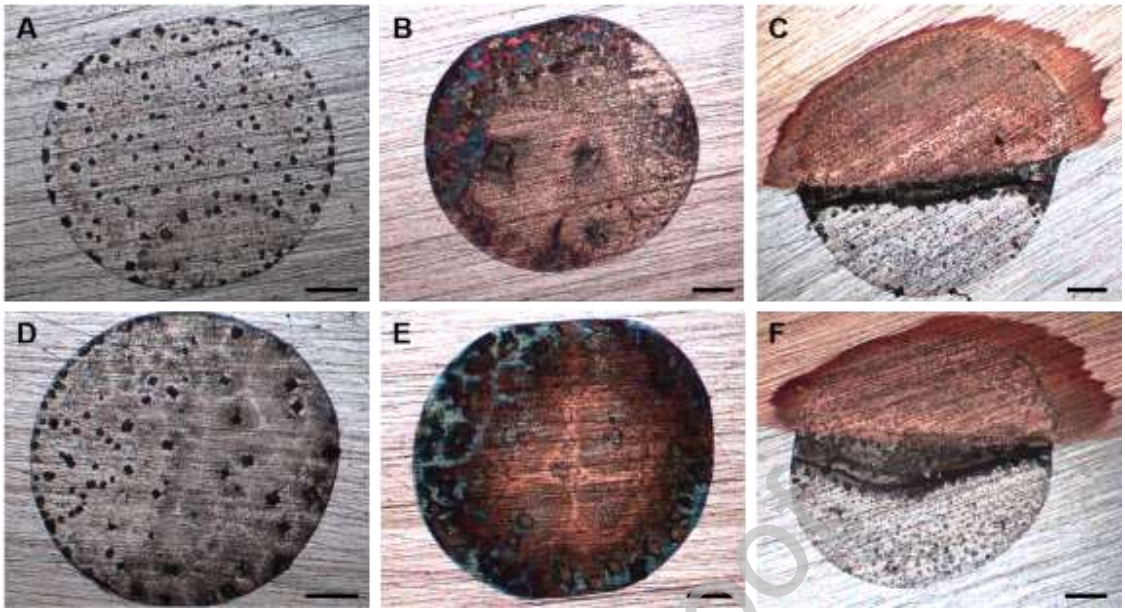

Figure 5: Optical micrographs after measurements in air of the droplet footprint created at open circuit potential (A-C), and after polarization measurements (D-F) on Al alloy (A and D), pure Cu (B and E), and the interface (C and F). All footprints on Cu and the Al alloy are relatively circular. At the interface of the two metals, the wetted surface area is dynamic at OCP and during PDP measurements. The scale bars represent 200 µm.

Journal Pre-proof

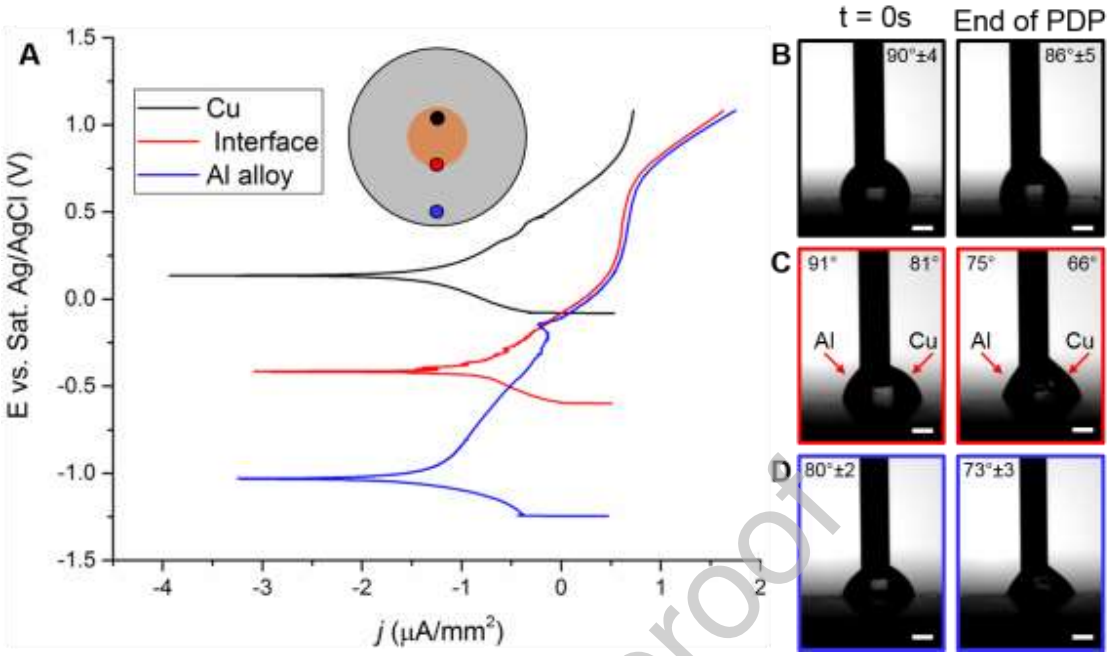

Figure 6: A) Representative potentiodynamic polarization curves obtain for each region investigated in an argon (deaerated) environment: pure copper (black), Al alloy (blue), and at the interface of the two metals (red). A schematic is added aid in the visualization of the sampled regions. B-D) Corresponding optical images of the salt droplets taken using the goniometer system before and after PDP measurements. Unlike the measurements performed in air, the droplets are symmetrical on all regions investigated as indicated by the similar water contact angles measured. Scale bars represent 500 μm.

Journal Pre-proof

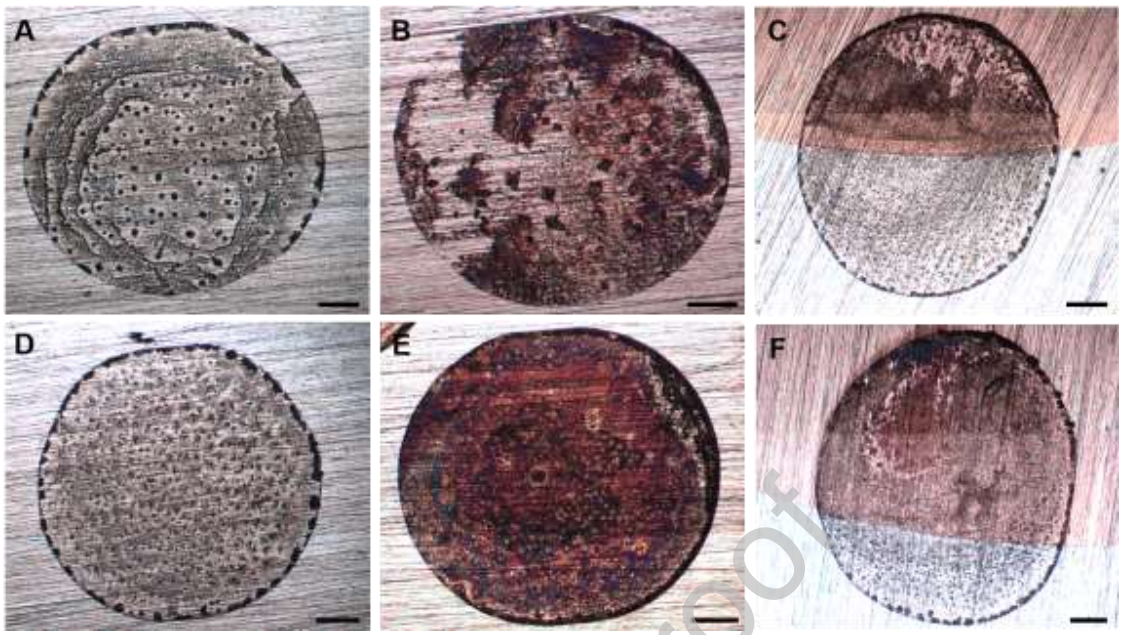

Figure 7: Optical micrographs after measurements in argon of the droplet footprint created at open circuit potential (A-C), and after polarization measurements (D-F) on Al alloy (A and D), pure Cu (B and E), and the interface (C and F). All footprints are relatively circular. Unlike measurements performed in air, it can be seen that the wetted surface area is constant at OCP and during PDP measurements. The scale bars represent 200 µm.

Journal Pre-proof

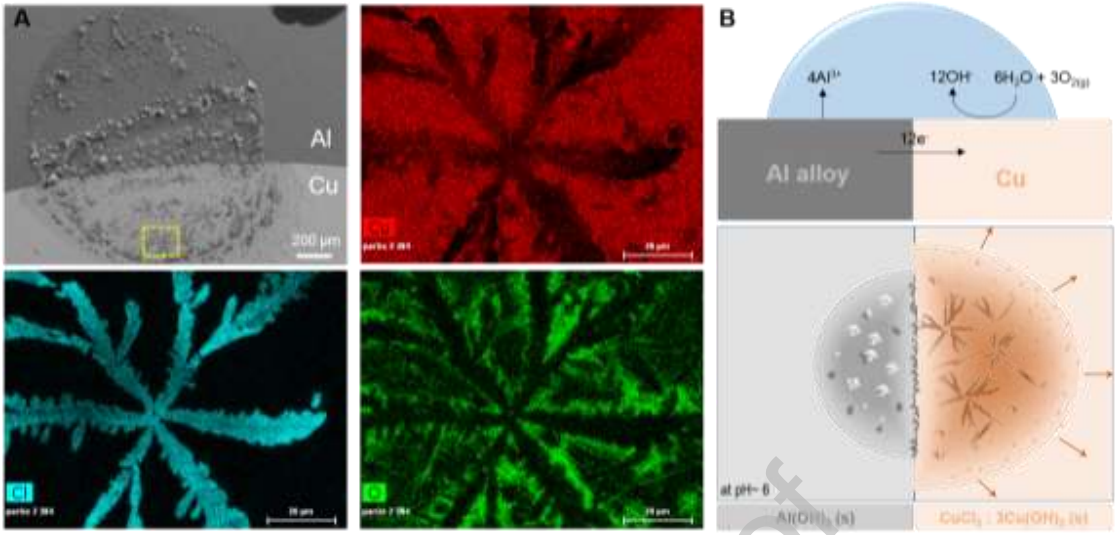

Figure 8: A) Shows electron micrographs and chemical composition maps of the corrosion product formed on Cu. B) Schematic of the proposed mechanism causing wettability changes in air. Surrounding oxygen present adjacent of the droplet diffuses into the droplet at the edges, causing the expansion of the surface area on Cu. This oxygen reduces on the surface of the Cu, which is supported by the oxidation of Al.

Journal Pre-proof